Research Paper

Distance Dependence of Gold-Enhanced Upconversion luminescence in Au/SiO$_2$/Y$_2$O$_3$:Yb^{3+}, Er^{3+} Nanoparticles

W. Ge[1], X. R. Zhang[2], M. Liu[1, ✉], Z. W. Lei[1], R. J. Knize[3] and Yalin Lu[1,2,3, ✉]

1. CAS Key Laboratory of Materials for Energy Conversion; Department of Materials Science and Engineering, University of Science and Technology of China, Hefei 230026, P. R. China;
2. Hefei National Laboratory for Physical Sciences at the Microscale, Hefei 230026, P. R. China.
3. Laser Optics Research Center, Physics Department, United States Air Force Academy, CO 80840, USA.

✉ Corresponding author: liumin1106@ustc.edu.cn, yllu@ustc.edu.cn, yalin.lu@usafa.edu.

Abstract

We report a localized surface plasmon enhanced upconversion luminescence in Au/SiO$_2$/Y$_2$O$_3$:Yb^{3+},Er^{3+} nanoparticles when excited at 980 nm. By adjusting the silica spacer's thickness, a maximum 9.59-fold enhancement of the green emission was obtained. Effect of the spacer distance on the Au-Y$_2$O$_3$:Yb^{3+}, Er^{3+} green upconversion mechanism was numerically simulated and experimentally demonstrated. In theory for radiative decay and excitation rates, they can be largely enhanced at the spacer thicknesses of less than 70 and 75 nm, respectively, and the quenching can be caused by the non-radiative energy transferring at the distance of less than 55 nm.

Key words: Plasmon coupling, Core/spacer/shell, Rare earth, Luminescence, Decay trace.

Introduction

Fluorescence imaging using nanoparticles could be a powerful tool for both biological studies and clinical medical applications due to its potential of convenience, high resolution and high sensitivity [1]. Conventional biolabels for imaging mainly include organic dyes and quantum dots (QD). Unfortunately, organic dyes are normally vulnerable to chemical and metabolic degradation, limiting the long-term cell tracking in experiments. On the other hand, possible toxicity of residual QDs has been a wide and persistent concern, even though much work has been underway to synthesize less harmful QDs or to enhance their biocompatibility [2]. Furthermore, excitation of these traditional biolabels usually requires the use of high energy photons such as UV radiation, which actually results in a series of drawbacks: (i) low signal-to-noise ratio due to the significant auto-fluorescence from biological samples under UV irradiation, (ii) low penetration depth due to the considerable absorption and scattering effects for short

wavelength photons, and (iii) possible severe photo-damage on cells and even the cell death further caused by the long-term irradiation of such high energy photons [3]. Therefore, it is desirable to obtain new fluorescent biolabels that can be excited by lower energy infrared (IR) light, which will be much safer to human body and can penetrate into tissues as far as several inches. Upconversion luminescent nanoparticles, which can convert long wavelength radiation into short wavelength fluorescence via a two- or multi-photon mechanism, are emerging as a new class of fluorescent biolabels [4-7]. Unfortunately, this upconversion process in general associates with low efficiency.

Past researches have been extensively focused on enhancing upconversion luminescence by using metallic nanoparticles or nanostructures [8-12]. In 2009, Yan et al obtained 2.3 and 3.7-fold enhancement for green and red emissions in NaYF$_4$:Yb^{3+}, Er^{3+} nanocrystals by attaching them to Ag nanowires [13]. In

2010, Benson et al. demonstrated a 3.8-fold upconversion enhancement by catching a single $NaYF_4$:Yb^{3+}, Er^{3+} nanocrystal adjacent to an Au nanoparticle [14]. Zhang et al. showed that the enhancement factor of approximately 2.6 can be achieved by attaching $NaYF_4$: Yb^{3+},Tm^{3+} hexaplate nanocrystals to gold nanoparticles [15], and a 4-fold upconversion enhancement is also found in Ag/Y_2O_3:Er^{3+} nanoparticles [16]. Most impressively, a five-fold overall enhancement of upconversion emission was demonstrated in $NaYF_4$: Yb^{3+}, Er^{3+} nanocrystals when coupled them with gold island films [17]. However, all previously reported enhancement factors were less than 5-fold, and in many cases, quenching was unavoidable [18, 19], mainly due to the following reasons: (1) frequency mismatching between the localized plasmon resonance (usually determined by the used metal, their shape, size, the dielectric environment, and the spacer distance) and the used emission/excitation light, (2) a competition of a few processes including a increase of the excitation rate by the local field enhancement (LFE) [20], an enhancement of radiative decay rate by the surface plasmon-coupled emission (SPCE) and quenching that reduces the efficiency caused by the non-radiative energy transferring (NRET) from the upconversion material to the metal surfaces [21,22], all of which will be greatly dependent on the spacing distance between the upconversion material and the metal [23-26].

In this research, we have adopted a series of strategies with a goal to further enhance the upconversion luminescence: 1) instead of using Ag in many previous researches, we selected Au nanoparticle, considering a better overlapping between Au's intrinsic plasmon resonance and the visible emission; 2) the most widely used sensitizer Yb^{3+} was co-doped with the activator Er^{3+}, first-timely in Y_2O_3 as shell to cap onto the SiO_2 spacer and the Au core in the $Au/SiO_2/Y_2O_3$:Yb^{3+},Er^{3+} (core/spacer/shell) nanostructure to be synthesized in this work. This was intended to increase the absorption cross section of Er^{3+} ions around 980nm; 3) the SiO_2 spacer thickness between Au and Y_2O_3:Yb^{3+}, Er^{3+} was intentionally changed with a goal to optimize the core/spacer/shell structure, and also to compare with the previous results [16]. In our results, a maximum 9.59-fold enhancement of green emission was ob-

tained in ~30 nm $Au/SiO_2/Y_2O_3$:Yb^{3+},Er^{3+} nanoparticles with an optimized distance, and the distance's effect on the excitation rate, the radiative decay rate and the NRET were also simulated using a 3D-comsol in details, which would help us to further understand the enhancement process.

Experimental and characterizations

Synthesis of gold nanoparticles

Gold Nanoparticles were prepared using the method introduced by Frens [27]. A mean diameter of 30 nm Au nanoparticles were prepared by rapidly injecting a sodium citrate solution (1.3 mL, 38.8mM) into a boiling $HAuCl_4$ aqueous solution (100 mL, 0.3 mM) under vigorous stirring. After refluxing for 15 min., product was cooled to room temperature.

Synthesis of Au/SiO$_2$ nanoparticles

By a modified Stöber method [28], the Au/SiO_2 nanoparticles were synthesized. The freshly prepared gold colloid solution (10 mL) was added to isopropanol (40 mL) in a 100 mL conical flask. Under vigorous stirring, ammonia (2 mL, 28~30%) and tetraethoxysilane (TEOS) were subsequently added until a homogeneous solution was formed. After stirring for 8h, the product was separated by centrifugation at 6000 rpm for 15 min. and washed with water until pH=7.

Synthesis of Au/SiO$_2$/Y$_2$O$_3$:20at%Yb^{3+},2at%Er^{3+} (20/2%) nanoparticles

The final product was synthesized via homogeneous precipitation and calcination [29]. The as-prepared 0.05g Au/SiO_2 nanoparticle was dissolved in 100 mL deionized water. After ultrasoniced for 30 min., 1.78 mL (0.1M) $Y(NO_3)_3$, 0.20 mL (0.1M) $Yb(NO_3)_3$, 0.02 mL (0.1M) $Er(NO_3)_3$ solutions and 2.7g urea were subsequently added to the solution, then stirring 30 min. until uniform dispersion. The solution was heated to 80℃ for 5h with continuous stirring, then isolated by centrifugation and washed three times with water and ethanol. The final product was obtained after dried under vacuum at 80℃ for 12h, and calcined for 3h at 800℃. Figure 1 shows the detailed synthesis procedure of the $Au/SiO_2/Y_2O_3$:Yb^{3+}, Er^{3+} nanoparticles.
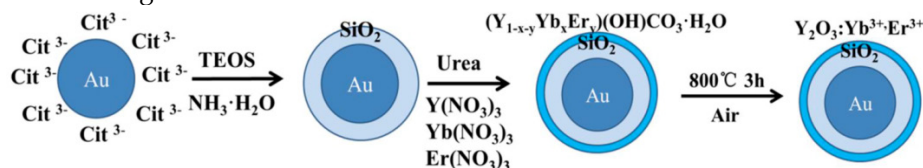
Figure 1. Synthesis procedure of the $Au/SiO_2/Y_2O_3$:Yb^{3+},Er^{3+} nanoparticles.

Synthesis of Y_2O_3:Yb^{3+}, Er^{3+} (20/2%) hollow nanoparticles

The Y_2O_3:Yb^{3+}, Er^{3+} hollow nanoshells were synthesized by using NaOH solution (5M) to etch silica in the SiO_2/Y_2O_3: Yb^{3+}, Er^{3+} nanoparticles.

Characterization of physical properties

The sizes and morphologies of all samples were observed by JEOL JEM-2011 transmission electron microscope (TEM) under a working voltage of 200 kV, as well as the EDX spectrum. The phase composition and crystallinity of the samples were characterized by XRD (Philips x'pert diffractometer employing Cu Kα radiation (λ=1.5405Å). Ultraviolet-visible-near infra-red (UV-Visible-NIR) absorption spectra were recorded with a Shimadzu SolidSpec-3700.

The upconversion emission spectra were recorded by use of Zeiss CLSM 710 confocal microscopy with a 100x plan-Apochromat objective (1.4 oil) equipped with a 980nm laser. All Au/SiO_2/Y_2O_3:Yb^{3+}, Er^{3+} samples with different spacer thicknesses were prepared in the same concentration in ethanol solution. We then spun 20μL from the bulk solution on a cover glass substrate, in this effort we could suggest all the samples have the same concentration. The upconversion luminescence data of such nanoparticles was analyzed as follows: Firstly, we randomly choose a luminescent area of 84.85μm×84.85μm from the full image of total upconversion luminescence. Secondly, we calculated the emission intensity per μm² from the selected area. This process was repeated a few times on different selected area positions, and then we average the emission intensity with the repeated times. Finally, this averaged emission intensity per μm² was multiplied with the superficial area of a single core/spacer/shell nanoparticle, and then we obtained the approximate upconversion emission from a single nanoparticle. This entire averaging process is statistically meaningful, and is necessary in our work because the setup we used cannot distinguish a single nanoparticle.

Results and discussion

The nanoparticles were characterized by TEM, EDX, XRD and HRTEM, as shown in Figure 2. Figure 2(a) shows a typical TEM image of the samples in which well-dispersed Au nanoparticles with an average size of 30 nm can be clearly seen. After the surface modification with a ~40nm thick SiO_2 dielectric spacer, the Au/SiO_2 becomes more uniform than before and highly mono-dispersed (Figure 2(b)). Then, a layer of ~12nm Y_2O_3: Yb^{3+},$Er^{3+}$was coated on the Au/SiO_2 surface (Figure 2(c)), which can be demon-

strated by the energy-dispersive X-ray microanalysis (EDX, Figure 2(d)) and X-ray diffraction (XRD, Figure 2(e)) patterns. A HRTEM image of Y_2O_3:Yb^{3+},Er^{3+} layer indicates the adjacent lattice fringes distance of 0.306nm, which can be assigned to the {222} crystal plane of the Y_2O_3 *bcc* phase (the insert of Figure 2(c)). The XRD patterns show well-defined peaks, indicating the high crystallinity of the as-prepared nanoparticles. Except the hollow Y_2O_3:Yb^{3+}, Er^{3+} (Figure 4(a)), all of the patterns show Au characteristic peaks with a *fcc* structure according to the PDF 04-0784 [Fm-3m (225)]. Because of the amorphous nature of the SiO_2 layer, there are no corresponding diffraction peaks. The Au/SiO_2/Y_2O_3:Yb^{3+}, Er^{3+} shows Y_2O_3 characteristic diffraction peaks indicating a cubic structure with a space group Ia-3(206) (PDF 01-0831), and the similar diffraction peaks also exist in the hollow Y_2O_3:Yb^{3+}, Er^{3+} patterns. Besides, TEM images of all the ~30nm Au/SiO_2 and ~30nm Au/SiO_2/Y_2O_3:Yb^{3+}, Er^{3+} nanostructures with different silica thicknesses were shown in Figure 3, which indicated that the thickness of Y_2O_3 shells are about 12 nm in all the samples.

In order to investigate the distance-dependence of metal-enhanced upconversion luminescence in Au/SiO_2/Y_2O_3:Yb^{3+},Er^{3+}nanoparticles with different SiO_2 thicknesses. The samples were measured by the Zeiss LCSM 710 confocal microscopy with a 100× plan-Apochromat objective (1.4oil) equipped with a 980nm laser. There are two main characteristic emission bands observed in Figure 4(a), corresponding to $^2H_{11/2}$/$^4S_{3/2}$-$^4I_{15/2}$ (green emission at ~524nm, ~549 nm) and $^4F_{9/2}$ -$^4I_{15/2}$ (red emission at ~665 nm) radiative transitions, respectively. Here, we defined a parameter EF_{green} (enhancement factor for green emission) and EF_{red} (enhancement factor for red emission) by dividing integrated fluorescence intensities of Au/SiO_2/Y_2O_3:Yb^{3+}, Er^{3+} nanoparticles by those of hollow Y_2O_3:Yb^{3+}, Er^{3+} nanoshells in the range of 500-560nm and 650-750 nm, respectively. In contrast to hollow Y_2O_3:Yb^{3+}, Er^{3+}nanoparticles, the green emission intensity of all core/spacer/shell nanoparticles is enhanced (EF_{Green}>1) (Figure 4(b)) and the corresponding red emissions of all samples are quenched (EF_{red}<1), which is attributed to the surface plasmon resonance frequency of Au nanoparticles having strong overlap with green emission band (Figure 4(c)), that is, an increase in emission rate by surface plasmon coupled emission (SPCE). SPCE is characterized by the increase of upconversion intensity accompanied by a decrease in the lifetime of upconversion nanoparticles located in the proximity of the metallic nanostructures. Therefore, decay curves of samples with and without Au core (Y_2O_3:Yb^{3+}, Er^{3+} hollow shell) have been also carried out. As shown in Figure

5, Au/SiO$_2$/Y$_2$O$_3$:Yb^{3+}, Er^{3+} nanoparticles exhibit shorter lifetime compared with the corresponding Y$_2$O$_3$:Yb^{3+}, Er^{3+} hollow shell, which supply direct proof for the conclusion that the enhancement originates from the increased emission rate. With the increase of SiO$_2$ thickness, EF$_{Green}$ increased and reached the maximum 9.59 when SiO$_2$ thickness is ~40 nm, and the ratio of green to red emission I$_{(G/R)}$ tracks well with the EF$_{Green}$ across the range of SiO$_2$ spacers, demonstrating a preferential enhancement of the green emission band. As mentioned in the introduction, the metal-enhanced/quenching fluorescence resulted from a competition of processes including an increase of excitation rate by LFE [20], an enhance-

ment of radiative decay rate by surface plasmon-coupled emission (SPCE) and the quenching caused by NRET from upconversion materials to metal surfaces [21, 22]. Near the metal surface, the upconversion intensity fall rapidly as the NRET from the emitters to the metal occurred. With the increase of the distance, SPCE and LFE became dominant and the EF reached the maximum at about 40 nm. Because the enhancement of emission and excitation rate cause by SPCE and LFE is proportion to the square of localized electric field, and the electric field decreased with the distance increase, the upconversion luminescence became weaker beyond the 40 nm distance.
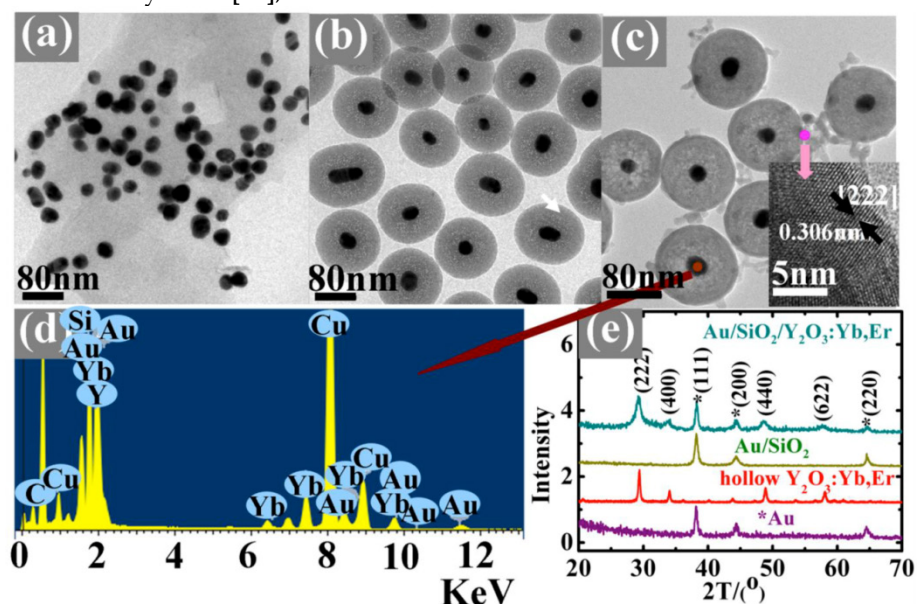

Figure 2. TEM images of (a) ~30nm Au (b) ~30nm Au/~40nmSiO$_2$ (c) ~40nmAu/~40nmSiO$_2$/~10nmY$_2$O$_3$:Yb^{3+},Er^{3+} (the insert is HRTEM image of lattice fringes of the Y$_2$O$_3$:Yb^{3+}, Er^{3+} layer) (d) EDX in a selected area of Au core and (e) XRD patterns of discussed samples (* represents Au diffraction peaks).
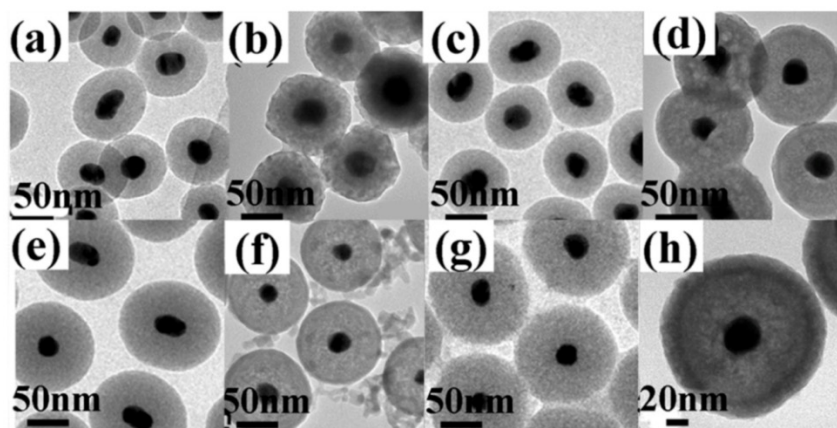
**Figure 3.** TEM images of (a) ~30nmAu/~25nmSiO$_2$; (b) ~30nmAu/~25nmSiO$_2$/~12nmY$_2$O$_3$:Yb^{3+}, Er^{3+}; (c) ~30nmAu/~30nmSiO$_2$; (d) ~30nmAu/~30nmSiO$_2$/~12nmY$_2$O$_3$:Yb^{3+},Er^{3+}; (e) ~30nmAu/~40nmSiO$_2$; (f) ~30nmAu/~40nmSiO$_2$/~12nmY$_2$O$_3$:Yb^{3+},Er^{3+}; (g) ~30nmAu/~45nmSiO$_2$; and (h) ~30nmAu/~45nmSiO$_2$/~12nmY$_2$O$_3$:Yb^{3+},Er^{3+}.
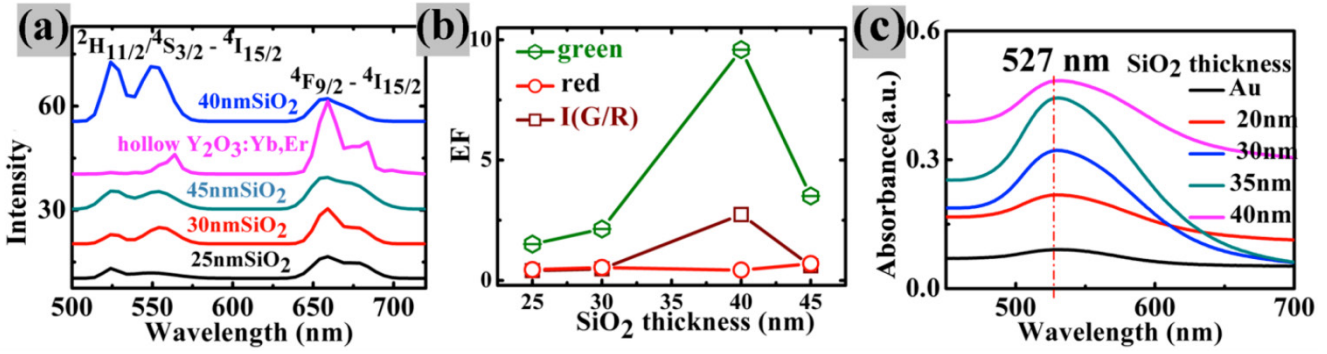
Figure 4. (a) The upconversion spectra in $Au/SiO_2/Y_2O_3:Yb^{3+},Er^{3+}$ nanoparticles with different SiO_2 thickness and the hollow $Y_2O_3:Yb$, Er (b) the plots of EF_{green}, EF_{red} and $I_{(G/R)}$ verse silica thickness (the integral of green emission intensity from 500nm to 560nm, the integral of red emission intensity from 650nm to 750nm); (c) UV-VIS absorption spectra of all the discussed samples.
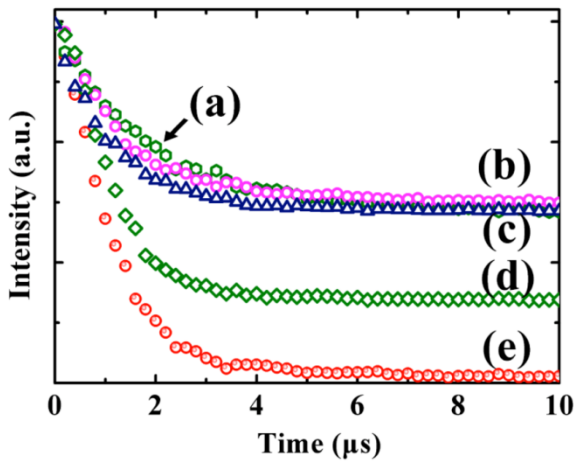

Figure 5. Decay curves for (a) $Y_2O_3:Yb^{3+},Er^{3+}$ hollow shells; (b)$Au/\sim45nmSiO_2/Y_2O_3:Yb^{3+},Er^{3+}$; (c)$Au/\sim40nmSiO_2/Y_2O_3:Yb^{3+},Er^{3+}$; (d)$Au/\sim30nmSiO_2/Y_2O_3:Yb^{3+},Er^{3+}$ and (e)$Au/\sim25nmSiO_2/Y_2O_3:Yb^{3+},Er^{3+}$ nanoparticles.

To understand deeply the distance-dependence of upconversion luminescence in $Au/SiO_2/Y_2O_3:Yb^{3+}$, Er^{3+} nanoparticles, the electric field enhancement factor $E'=|E_{gold}|/|E_o|$, where E_{gold} and E_o were the electric field with and without gold, was calculated by 3D-comsol, as presented in Figure 6. We studied a very general case by 3D-comsol: the Au nanoparticles were imbedded in a homogeneous, lossless SiO_2 medium, supposing the Au nanosphere is small as compared to the light wavelength. In Figure 6, d is the distance to the surface of Au nanospheres. The wavelength-dependence of electric field is similar with the measured absorption spectra of Au nanoparticles (see Figure 4(c)), and the greatest electric field strength was found to 8.9 at 525 nm. With the increase of d, the electric field falls rapidly, and near to unity at $d=90$ nm. The detailed unit-less parameters: the electric field enhancement factor at 549 nm and 980 nm (E'_{549nm}

and E'_{980nm}), and the overall enhancement factor of emission intensity at 549 nm, L_{549nm}, are listed in Table 1.

Table 1. The detailed list of the electric filed enhancement factor at 549 nm and 980 nm (E_{549nm} and E_{980nm}) and enhancement factor at 549 nm (L_{549nm}) for the $Au/SiO_2/Y_2O_3:Yb,Er$ nanoparticle.

d(nm)	25	30	40	45
E'_{549nm}	1.82	1.68	1.49	1.37
E'_{980nm}	1.20	1.16	1.11	1.07
L_{549nm}	1.51	2.14	9.59	3.51

The enhancement factor in the excitation (L_{ex}) and emission (L_{em}) rates as a funtion of the distance between Au and $Y_2O_3:Yb^{3+},Er^{3+}$ (d) could be expressed as [30]:

$$L_{ex}(d) = L_{ex}(d=0) \exp(-d/R_{ex}) + 1 \qquad \ldots(1)$$

$$L_{em}(d) = L_{em}(d=0) \exp(-d/R_{em}) + 1 \qquad \ldots(2)$$

R_{em} and R_{ex} is the characteristic distance over which $L_{em}(d=0)$ and $L_{ex}(d=0)$ decrease to 1/e exponentially, respectively.

The enhancement factor of excitation and emission rate by surface-plasmon-coupled emission is also proportional to the square of corresponding electric field enhancement [26]. Hereby, we analyzed our experimental upconversion intensity at 549 nm at various distance from the plasoninc metal-nanostructured surface. By fitting the experimental data with equation 1 and equation 2, the values of the free parameters $L_{em}(d=0)=5.7$, $L_{ex}(d=0)=1.3$, $R_{em}=16.2$ nm and $R_{ex}=23.9$ nm were obtained. Near the metal surface,

the fluorescence intensity fall rapidly due to non-radiative energy transfer from the fluorescence materials to the metal surface. A complete, classical theory of NRET has been published by Campion et al.. When $d \leq \lambda$, the expression of the unitless parameter quenching factor (Q) caused by NRET is as follows [31]:

$$Q = \omega_{ET}/\omega_R$$
$$= \{\omega_R \times Im[(\varepsilon_2 - \varepsilon_1)/(\varepsilon_2 + \varepsilon_1)] \times \lambda^3\} / [8\pi^3 \times (\varepsilon_1)^{3/2} \times 4d^3 \times \omega_R]$$
$$= \{Im[(\varepsilon_2 - \varepsilon_1)/(\varepsilon_2 + \varepsilon_1)] \times \lambda^3\} / [32\pi^3 \times (\varepsilon_1)^{3/2} \times d^3]$$
$$\ldots(3)$$

Where ω_{ET} is nonradiative rate, ω_R is the radiative rate constant, λ is the emission wavelength; $\varepsilon_1(549nm)=1.46$, is the dielectric constant of the spacer layer, and $\varepsilon_2(549nm)=0.306+2.88i$, is the complex dielectric constant of the metal [32].

The enhancement of excitation and radiative decay rate (L_{ex}, L_{em}) and the quenching factor by NRET (Q) are plotted as a function of Au-Y_2O_3 nanoparticle distance, as shown in Figure 7. It is apparent from distance-dependent plot that the radiative decay rate could be enhanced even at a distance of ~0 nm, and the enhanced excitation takes place below 75 nm. The quenching factor by NRET (Q) decreased rapidly as the distance increased, and near to L_{em} and L_{ex} at a distance of 55 nm.
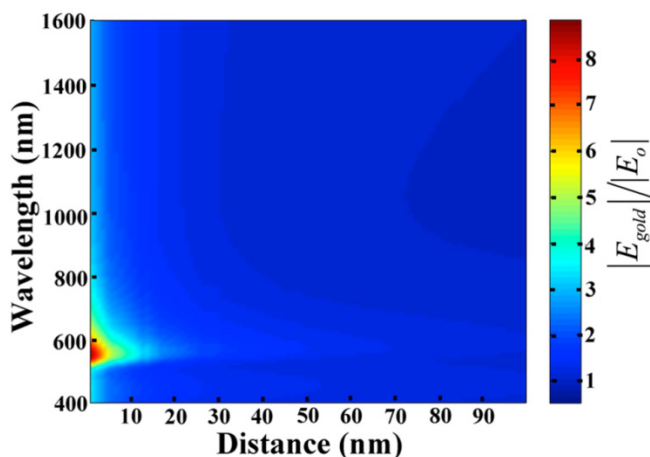

Figure 6. Electric field enhancement (E) dependence as a function of the wavelength and distance to a ~30nm diameter Au nanoparticle surface.
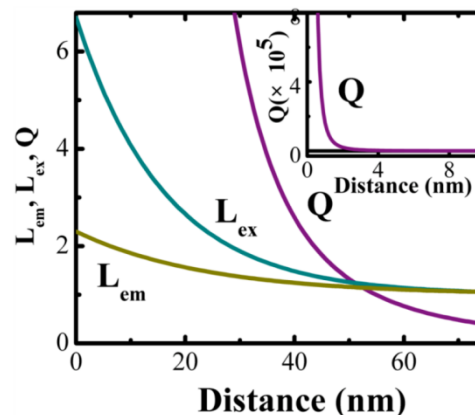

Figure 7. Changing of excitation rate $L_{ex}(S^{-1})$ and radiative decay rate $L_{em}(S^{-1})$, and the quenching factor by NRET (Q), as a function of the spacing distance from the metal surface.

Conclusions

In conclusion, plasmon-enhanced upconversion luminescence was observed in Au/SiO_2/Y_2O_3:Yb^{3+},Er^{3+} nanoparticles. With the increase of silica dielectric thickness, the green emission intensity increased and reached a maximum 9.59-fold enhancement when silica thickness is ~40 nm, which attributed to the competition of non-radiative energy transfer (NRET) from Y_2O_3:Yb^{3+}, Er^{3+} to Au core, enhancement of radiative decay rate by surface plasmon-coupled emission (SPCE) and an increase of excitation rate by local field enhancement (LFE). The distance's effect on the enhancement factor of radiative decay and excitation rate and quenching factor by NRET was simulated. The radiative decay rate could be enhanced even at a distance of 70 nm, and the enhanced excitation rare takes place below 75 nm. The quenching factor by NRET (Q) decreased rapidly with the distance increase, and is near to L_{em} and L_{ex} at a distance of 55 nm.

Acknowledgment

Competing Interests

The authors have declared that no competing interest exists.

References

1. Grunwald D, Singer R. In vivo imaging of labelled endogenous beta-actin mRNA during nucleocytoplasmic transport. Nature. 2010; 467: 604-607.
2. Derfus A, Chan W, Bhatia S. Probing the cytotoxicity of semiconductor quantum dots. Nano Lett. 2004; 4: 11-18.
3. Jalil R, Zhang Y. Biocompatibility of silica coated NaYF$_4$ upconversion fluorescent nanocrystals. Biomaterials. 2008; 29: 4122-8.
4. Wang F, Han Y, Lim CS, Lu Y, Wang J, Xu J, Chen H, Zhang C, Hong M, Liu X. Simultaneous phase and size control of upconversion nanocrystals through lanthanide doping. Nature. 2010; 463: 1061-5.
5. Chen GY, Ohulchanskyy TY, Liu S, Law W, Wu F, Swihart MT. Core/shell NaGdF$_4$: Nd^{3+}/NaGdF$_4$ nanocrystals with efficient near-infrared to near-infrared downconversion photoluminescence for bioimaging applications. ACS Nano. 2012; 6: 2969-77.
6. Chen GY, Ohulchanskyy TY, Kachynski A, Agren H, Prasad PN. Intense visible and near-infrared upconversion photoluminescence in colloidal LiYF$_4$:Er^{3+} nanocrystals under excitation at 1490 nm. ACS Nano. 2011; 5: 4981-6.
7. Wang C, Cheng L, Xu H, Liu Z. Towards whole-body imaging at the single cell level using ultra-sensitive stem cell labeling with oligo-arginine modified upconversion nanoparticles. Biomaterials. 2012; 33: 4872-81.
8. Aisaka T, Fujii M, and Hayashi S. Enhancement of upconversion luminescence of Er doped Al$_2$O$_3$ films by Ag island films. Appl. Phys. Lett. 2008; 92: 132105-7.
9. Esteban R, Laroche M, and Greffet JJ. Influence of metallic nanoparticles on upconversion processes. J.Appl. Phys. 2009; 105: 033107-16.
10. Ming T, Zhao L, Yang Z, Chen H, Sun LD, Wang J, Yan CH. Strong polarization dependence of plasmon-enhanced fluorescence on single gold nanorods. Nano Lett. 2009; 9: 3896-3903.
11. Priyam A, Idris NM, and Zhang Y. Gold nanoshell coated NaYF4 nanoparticles for simultaneously enhanced upconversion fluorescence and darkfield imaging. J. Mater. Chem. 2012; 22: 960-5.
12. Lu Y and Chen X. Plasmon-enhanced luminescence in Yb^{3+}: Y$_2$O$_3$ thin film and the potential for solar cell photon harvesting. Appl. Phys. Lett. 2009; 94: 193110-2
13. Feng W, Sun LD, and Yan CH. Ag nanowires enhanced upconversion emission of NaYF$_4$:Yb,Er nanocrystals via a direct assembly method. Chem.Commun.2009; 29: 4393-5.
14. Schietinger S, Aichele T, Wang H, Nann T, and Benson O. Plasmon-enhanced upconversion in single NaYF$_4$:Yb^{3+}/Er^{3+} Codoped Nanocrystals. Nano Lett. 2010; 10: 134-8.
15. Zhang H, Li Y, Ivanov IA, Qu Y, Huang Y and Duan X. Plasmonic modulation of the upconversion fluorescence inNaYF$_4$:Yb/Tm hexaplate nanocrystals using gold nanoparticles or nanoshells. Angew. Chem. Int. Ed. 2010; 49: 2865-8.
16. Zhang F, Braun GB, Shi Y, Zhang Y, Sun X, Reich NO, Zhao D, and Stucky G. Fabrication of Ag@SiO$_2$@Y$_2$O$_3$:Er nanostructures for bioimaging: tuning of the upconversion fluorescence with silver nanoparticles. J. Am. Chem. Soc. 2010; 132: 2850-1.
17. Zhang H, Xu D, Huang Y, and Duan X. Highly spectral dependent enhancement of upconversion emission with sputtered gold island films. Chem. Commun. 2011; 47: 979-81.
18. Boyer JC, Cuccia LA, Capobianco JA. Synthesis of colloidal upconverting NaYF4: Er3+/Yb3+ and Tm3+/Yb3+ monodisperse nanocrystals. Nano. Lett. 2007; 7: 847-52.
19. Vetrone F, Naccache R, Juarranz A, Fuente A, Rodriguez FS, Maestro LM, Rodriguez EM, Jaque D, Sole JG. Capobianco JA, Temperature sensing using fluorescent nanothermometers. ACS Nano. 2010; 4: 3254-8.
20. Lakowicz JR. Radiative decay engineering: biophysical and biomedical applications. Anal. BioChem. 2001; 298: 1-24.
21. Gryczynski I, Malicka J, Gryczyski Z, Lakowicz JR. Radiative decay engineering 4: experimental studies of surface plasmon-coupled directional emission. Anal. BioChem. 2004; 324: 170-182.
22. Campion A, Gallo AR, Harris CB, Robota HJ, Whitmore PM. Electronic-energy transfer to metal-surfaces-a test of classical image dipole theory at short distances. Chem. Phys. Lett. 1980; 73: 447-50.
23. Guillermo PA, Martina B, Ingo HS, Christian S, Anton K, Phil H, Robert S, Alexander M, Fernando DS, Tim L, Friedrich CS, and Philip T. Distance dependence of single-fluorophore quenching by gold nanoparticles studied on DNA origami. ACS Nano. 2012; 6: 3189-95.
24. Schneider G, and Decher G. Distance-dependent fluorescence quenching on gold nanoparticles ensheathed with layer-by-layer assembled polyelectrolytes. Nano Lett. 2006; 6: 530-6.
25. Akbay N, Lakowicz JR, and Ray K. Distance-dependent metal-enhanced intrinsic fluorescence of proteins using polyelectrolyte layer-by-layer assembly and aluminum nanoparticles. J. Phys. Chem. C. 2012; 116: 10766-73.
26. Kümmerlen J, Leitner A, Brunner H, Aussenegg FR, and Wokaun A. Enhanced dye fluorescence over silver island films: analysis of the distance dependence. Mol. Phys. 1993; 80: 1031-46.
27. Frens G. Controlled nucleation for regulation pf particle-size in monodisperse gold suspensions. Nature. 1973; 241: 20-22.
28. Lu Y, Yin YD, Li ZY, Xia YA. Synthesis and self-assembly of Au@SiO$_2$ core−shell colloids. Nano Lett. 2002; 2: 785-788.
29. Rosa ILV, Oliveira LH, Suzuki CK, Varela JA, Leite ER, Longo E. SiO$_2$-GeO$_2$ soot preform as a core for Eu$_2$O$_3$ nanocoating: synthesis and photophysical study. J Fluoresc. 2008; 18: 541-545.
30. Akbay N, Lakowicz JR, and Ray K. Distance-dependent metal-enhanced intrinsic fluorescence of proteins using polyelectrolyte layer-by-layer assembly and aluminum nanoparticles. J. Phys. Chem. C. 2012; 116: 10766-73.
31. Campion A, Gallo AR, Harris CB, Robota HJ, Whitemore PM. Electronic energy transfer to metal surfaces: a test of classical image dipole theory at short distances. Chem. Phys. Lett. 1980; 73: 447-9.
32. Lynch DW, and Hunter WR. Handbook of Optical Constants of Solids. New York: Academic Press. 1985: 274 -760.